

The Effect of Sulphate and Chloride Palladium Salt Anions on the Morphology of Electrodeposited Pd Nanoparticles and their Catalytic Activity for Oxygen Reduction in Acid and Alkaline Media

Jelena Golubović¹, Lazar Rakočević², Svetlana Štrbac^{1,*}

¹ ICTM-Department of Electrochemistry, University of Belgrade, Njegoševa 12, 11000 Belgrade, Serbia

² INS Vinča, Laboratory of Atomic Physics, University of Belgrade, Mike Petrovića Alasa 12-14, 11351 Belgrade, Serbia

*E-mail: sstrbac@tmf.bg.ac.rs

Received: 8 May 2022 / Accepted: 28 June 2022 / Published: 7 August 2022

Pd/GC electrodes were prepared by the electrochemical deposition of palladium on glassy carbon (GC) using PdSO₄ or PdCl₂ salts. As-prepared GC-supported Pd nanoparticles were characterized by X-ray photoelectron spectroscopy (XPS) and atomic force microscopy (AFM). XPS spectra revealed that the depositing palladium salt anion influences the oxidation state of the deposited Pd, while AFM images showed its effect on Pd nanoparticle size and coverage. The deposition from the PdCl₂ salt solution resulted in smaller palladium nanoparticles, but much higher GC surface coverage than from PdSO₄. The activity of Pd/GC electrodes towards oxygen reduction was examined in acid and alkaline media using the rotation-disc electrode. Among the different Pd/GC electrodes, the one prepared using PdCl₂ salt with the full Pd coverage has shown the best ORR activity. The ORR occurs through a 4e-series reaction mechanism like on polycrystalline palladium but exceeds its activity concerning the initial potential.

Keywords: Electrocatalysis; Electrochemistry; Glassy carbon; Oxygen reduction; Palladium

1. INTRODUCTION

Oxygen reduction reaction (ORR) is one of the most important and comprehensively studied cathodic fuel cell reactions. Among precious metals, platinum is the most active for ORR, but the activity of palladium having the most similar intrinsic features is next to it [1,2]. The structural effect on the kinetics of ORR on Pt single crystals of various orientations [3-5] and Pd low-index surfaces [6] was studied extensively. Besides, the ORR catalytic activity of polycrystalline platinum, Pt(poly) [7], and

palladium, Pd(poly) [8,9] were studied in detail. Due to the high cost of precious metals including palladium, savings in their consumption as electrodes in fuel cells is the utmost goal of great importance for commercial needs. That goal is achieved only when a small amount of precious metal(s) is used as a catalyst supported by a cheaper substrate. Among different types of ORR catalysts developed so far, Pd-based catalysts have attracted much attention in recent years, including supported alloys and different nanostructures, in which palladium combines with the other precious and non-precious metals [10-13].

There are many reports on ORR catalysts consisting only of palladium supported by various carbon materials, from dispersed Pd nanoparticles (NPs) [14-18] to thin films [19-21]. The ORR activity of Pd-based catalysts depends a lot on the surface morphology. Since the most active palladium single crystal is Pd(100) [3], the most active Pd nanoparticles would be those dominated by (100) orientation having a cubic structure [22-24]. The catalytic activity of cubic Pd nanoparticles on a carbon substrate showed higher activity when compared to spherical and octahedral palladium nanoparticles [23]. On the other hand, the ORR activity of Pd nanorods, having the facets of (110) orientation, is close to that of Pt and higher than that of conventional palladium NPs [25].

The preparation of Pd-based catalysts involves various methods [26-28], among which the widely exploited electrochemical deposition is an easy and quick way to prepare nanostructured palladium thin films [17, 29], Pd mesoparticles [30], nanoparticles, nanowires, and nanorods [25,26]. The deposit structure is very dependent on the type of anions originating from the depositing palladium salt. There are studies of the electrochemical deposition of palladium on a GC substrate electrode from commonly used Pd salt solutions containing either sulfate [31] or chloride ions [32-34]. In both cases, the morphology of the Pd deposit depends on the type of the basic depositing solution and depositing salt concentration and on the electrochemical parameters involving the deposition potential and time. As for the deposition potential, there is overpotential deposition (OPD) at the electrode potentials lower than those determined by the Nernst equation and underpotential deposition (UPD) at higher deposition potentials. The electrode potential dictates the rate of the deposition process, which is higher during OPD and lower during UPD, which in turn, determines the morphology of the deposit. That is illustrated in the detailed study on Pd deposition on carbon substrates using the depositing PdSO₄ salt solution [31], which resulted in the formation of one-dimensional (1D) nanowires, two-dimensional (2D) and three-dimensional (3D) nanoparticles, and thin films depending on the deposition conditions. The electrochemical deposition of Pd on a graphite electrode using PdCl₂ depositing salt occurs through 2D growth mode, which changes to 3D by shifting the electrode potential to more negative values [32]. Pd deposition on glassy carbon (GC) proceeds only through 3D island growth [35,36]. In contrast to 2D, the 3D structure is more porous and provides a larger electrochemically active surface [37]. So far synthesized 3D porous Pd nanostructures of different shapes and morphologies have a high surface roughness and active surface sites contributing thus to the improvement of ORR catalytic activity [38]. Also, by the electrochemical Pd deposition, the dendritic structures are obtained, the morphology of which is controlled by adjusting the deposition potential [39,40]. The dendritic structures of palladium obtained by the electrochemical Pd deposition on a pure Au electrode have higher ORR catalytic activity than the commercial Pt/C [41]. For catalysts formed by the electrochemical Pd deposition on GC, the oxygen reduction occurs through the 4e⁻ reaction pathway both in acid and alkaline solutions following the reaction mechanism similar to that on pure palladium [9,19,42].

In this work, we investigated the catalytic activity of Pd/GC electrodes for oxygen reduction reaction in acid and alkaline media. The preparation of Pd/GC electrodes involves the electrochemical deposition of palladium on the GC substrate from the depositing solutions containing two different Pd salts (PdCl₂ and PdSO₄·H₂O). Pd/GC electrodes are characterized using microscopic, spectroscopic, and electrochemical techniques. The activity of the prepared Pd/GC electrodes for ORR is investigated using standard electrochemical methods. The optimum deposition conditions are determined to prepare Pd/GC electrodes having the ORR activity even higher than bare Pd.

2. EXPERIMENTAL

2.1. Pd/GC electrodes preparation

Glassy-carbon discs, 5 mm in diameter (Alfa Aesar), mounted in a Teflon holder was used as substrate electrodes for electrochemical measurements, while GC disc, 7 mm in diameter was used for *ex-situ* surface characterization. Before each measurement, the GC electrode is mechanically polished, and cycled 10 times in deaerated 0.1 M HClO₄ solution in the potential range from 0.02 V to 1.22 V (*vs.* RHE), or in 0.1 M NaOH from 0.13 V to 1.33 V (*vs.* RHE). After each measurement, the electrode surface is cleaned from the previous deposit by potential cycling.

Pd/GC electrodes are prepared by the electrochemical deposition of Pd from PdSO₄ and PdCl₂ salts. Electrochemical deposition of Pd is performed using chronoamperometry (CA) technique. Palladium is deposited at a constant potential (*vs.* Ag/AgCl/3M KCl) from (1×10⁻⁴ M PdSO₄ ·2H₂O + 0.05 M H₂SO₄) and (1×10⁻⁴ M PdCl₂ + 0.05 M H₂SO₄) solutions for various times (further in the text denoted as the deposition time).

2.2. Characterization of Pd/GC electrodes

Atomic Force Microscopy (AFM) imaging is performed in a tapping mode using Multimode Quadrex SPM (Veeco Instruments, Inc.) with a silicon probe (Tip-Vista probe, T190R-25, 190 kHz cantilever with tip radius lower than 10 nm). Height and phase AFM images of as-prepared Pd/GC electrodes are recorded simultaneously over the same electrode surface area. Height AFM images provide information about surface topography including the size of the deposited Pd nanoparticles. Phase AFM images provide additional information about the coverage of the GC substrate with the deposited Pd nanoparticles, and the difference in Pd/GC surface chemical composition depending on the type of anion in the depositing Pd salt.

X-Ray Photoelectron Spectroscopy (XPS) spectra of as-prepared Pd/GC samples are recorded by SPECS Systems with XP50M X-ray source for Focus 500 and PHOIBOS 100/150 analyzer, and AlK α source (1486.74 eV) at a 12.5 kV and 32 mA at a pressure of 9 × 10⁻⁹ mbar. Survey spectra are recorded in the binding energy range of 0-1000 eV, and high-resolution spectra of C 1s, O 1s, Pd 3p, and Pd 3d photoelectron lines. The C 1s line at 284.8 eV is used as a reference for all peak positions. Spectra are analyzed by SpecsLab data analysis software and analyzed with CasaXPS software.

2.3. Electrochemical measurements

Electrochemical measurements are performed using Pine Instruments potentiostat AFCEBP1, and a standard three-electrode cell. Pd/GC electrodes are used as working, Pt wire as a counter, and Ag/AgCl (3 M KCl) as a reference electrode. All potentials are corrected relative to the reversible hydrogen electrode (RHE) ($E_{\text{RHE}} = E_{\text{Ag/AgCl (3M KCl)}} + 0.0592 \times \text{pH} + 0.209 \text{ V}$). Cyclic Voltammetry (CV) technique is used for the electrochemical characterization of the obtained electrodes in the deaerated 0.1 M HClO₄ and 0.1 M NaOH solutions. Linear Sweep Voltammetry (LSV) is used for the investigation of their electrocatalytic activity for the oxygen reduction reaction. ORR measurements are performed by the Rotating-Disc Electrode (RDE) method at different rotation rates, expressed in rotations per minute (rpm). Polarization curves for ORR on Pd/GC are recorded in the cathodic direction in the potential range from 0.97 V to 0.11 V in acid, and from 1.08 to 0.22 V in alkaline solution. Before each measurement, the electrode is held at a constant potential of 0.09 V in acid, and at 0.20 V in alkaline solution, to reduce the deposited palladium to the metallic state. Current densities are calculated related to the geometric surface area of the working electrodes (0.196 cm²). Electrochemically active surface areas and ORR specific activities are calculated for the most active Pd/GC electrodes as will be shown below.

2.4. Chemicals

The working solution is prepared using supra-pure HClO₄ (Merck) or NaOH pellets (Merck). Depositing solutions are prepared using PdSO₄·2H₂O and PdCl₂ (Alfa Aesar), supra-pure H₂SO₄ (Merck), and Milli-pure water. Solutions are deaerated using 99.9995 % N₂ (Messer), or oxygen saturated using 99.9995 % O₂ (Messer).

3. RESULTS AND DISCUSSION

3.1. Pd/GC electrodes preparation

Pd/GC electrode preparation involves the electrochemical deposition of Pd on the GC substrate electrode at three different applied potentials. Potentials are given relative to the reversible hydrogen electrode (RHE) for all electrochemical measurements. Taking into account that the standard equilibrium potential for Pd²⁺/Pd is 0.95 V [43], the calculated Nernst equilibrium potential for palladium deposition from both solutions (10⁻⁴ M Pd²⁺, pH 1) is 0.80 V. According to refs. [44,45], as a result of the electrodeposition of Pd onto Pt(111) and Au(111) using PdCl₂ and PdSO₄ salts, a pseudomorphic Pd monolayer is formed first in both cases. In the presence of chloride anions in the depositing solution, the formation of this monolayer occurs in the UPD region. On the other hand, in the presence of sulfate anions, it is kinetically hindered, and the Pd monolayer formation occurs in the OPD region. Accordingly, in this work, although the two depositing salts contain different anions, the presence of sulfate anions in the same depositing base solution hinders the UPD of Pd on GC in both cases, and the deposition at all chosen potentials occurs in the OPD region. It is worth noting that although PdCl₂ is

better dissolved in hydrochloric or perchloric acid than in the sulfuric acid base solutions, the aim of this work was to emphasize the influence of the depositing salt anion, which was the main reason to choose the same base sulfuric acid solution.

Figure 1 shows cyclic voltammograms (CVs) of the bare GC electrode in the base 0.05 M H₂SO₄ solutions containing either PdSO₄ or PdCl₂ depositing salts. The Pd deposition on GC proceeds with low current densities starting from the Nernst potential and with increasing current densities at lower potentials. Deposition occurs with a reasonably high current density at about 200 mV more positive potential when using PdCl₂ salt instead of PdSO₄.

Figure 1a shows CV of the bare GC in (1 × 10⁻⁴ M PdSO₄·2H₂O + 0.05 M H₂SO₄) solution recorded in the potential range from 1.07 V to 0.02 V. The shape of the CV curve does not change significantly during scanning in the cathodic direction from 1.07 V up to the potential of approx. 0.27 V, at which the palladium deposition begins. The current density further increases and reaches the maximum value at approx. 0.19 V. The appearance of this most prominent cathodic peak can be ascribed to the simultaneous Pd deposition and hydrogen adsorption on already deposited palladium nanoparticles since its position falls within the hydrogen UPD region. After that, the cathodic current first decreases to the potential of 0.09 V, then increases again due to the simultaneous palladium deposition and hydrogen evolution on the deposited palladium, in line with the observation for similar deposition conditions as described in ref. [31]. The deposition of palladium was performed at three different applied potentials chosen in the hydrogen UPD region: 0.26 V, coinciding with the beginning of the deposition; 0.19 V, at the hydrogen UPD peak; 0.09 V, the potential after which hydrogen evolution on the deposited Pd nanoparticles begins.

Figure 1b shows cyclic voltammograms of bare GC electrode in the depositing (1 × 10⁻⁴ M PdCl₂ + 0.05 M H₂SO₄) solution, recorded in the potential range from 1.27 V to 0.02 V. Palladium deposition begins at the potential of approx. 0.52 V, while the maximum current density is achieved at 0.42 V. It is supposed that the deposition occurs predominantly through palladium reduction from Pd²⁺ cations. The peak originating from the oxidation of the deposited palladium appears at 0.87 V. The appearance of a pair of cathodic/anodic peaks at 0.17 V/0.22 V, in the potential region of hydrogen UPD, can be ascribed to the simultaneous Pd deposition and hydrogen adsorption/desorption on already deposited Pd nanoparticles. The increase of the current density at potentials lower than 0.07 V is ascribed to the hydrogen evolution at the deposited Pd nanoparticles. Like in the previous case, the deposition of palladium was performed at different applied potentials: 0.47 V, at the beginning of Pd deposition; 0.42 V, and 0.25 V at the hydrogen UPD peak.

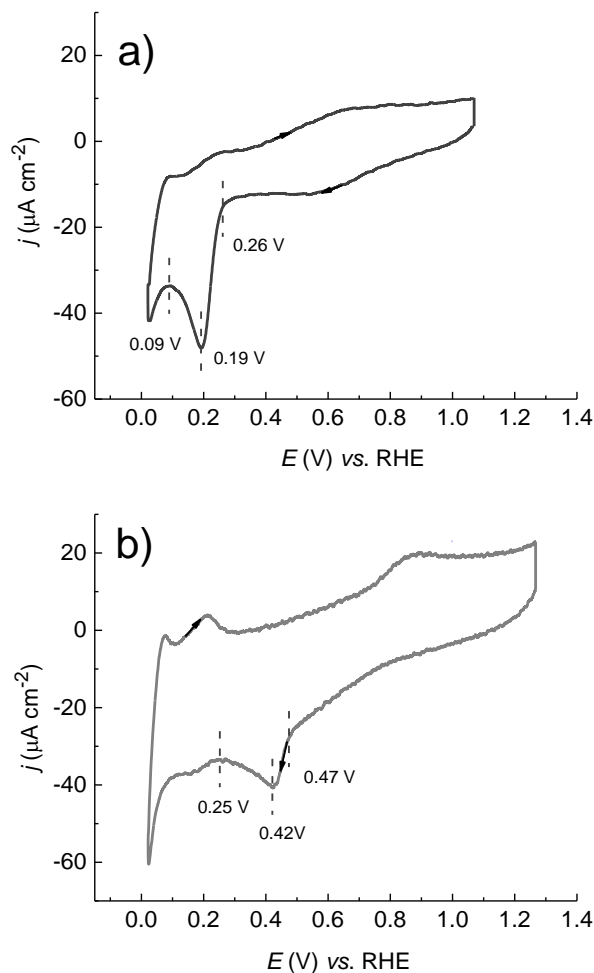


Figure 1. Cyclic voltammograms showing Pd deposition on GC electrode from different depositing solutions: a) (1×10^{-4} M $\text{PdSO}_4 \cdot 2\text{H}_2\text{O}$ + 0.05 M H_2SO_4); b) (1×10^{-4} M PdCl_2 + 0.05 M H_2SO_4). Scan rate 50 mV s^{-1} .

By varying the deposition time (10, 15, 30, and 60 min) for each of the three chosen deposition potentials, different Pd/GC electrodes are obtained. For each of them, a preliminary check of their ORR activity was performed. It was found that in both cases when Pd/GC electrodes were obtained using PdSO_4 or PdCl_2 salt, the best ORR activity was obtained when the deposition was performed at the lowest cathodic potential and for the deposition time of 30 minutes. Therefore, the AFM and XPS characterization, as well as the CV characterization and ORR activity measurements using the RDE technique in acid and alkaline electrolytes will be presented only for the most active Pd/GC electrodes. As shown below, the Pd/GC electrodes obtained after the deposition at 0.25 V from (1×10^{-4} M PdCl_2 + 0.05 M H_2SO_4) have shown the best activity for ORR.

3.2. AFM imaging of the Pd/GC

Figure 2 shows the height and phase AFM images of the Pd/GC surface, prepared by 30 min Pd deposition from (1×10^{-4} M $\text{PdSO}_4 \cdot 2\text{H}_2\text{O}$ + 0.05 M H_2SO_4) at a constant potential of 0.09 V. The height

AFM image, Figure 2a, showing the surface topography, reveals robust Pd nanoparticles randomly distributed over the GC substrate. Cross-section along the line indicated in the image, Figure 2b, shows that the lateral size of individual and agglomerated Pd nanoparticles ranges from 50–200 nm.

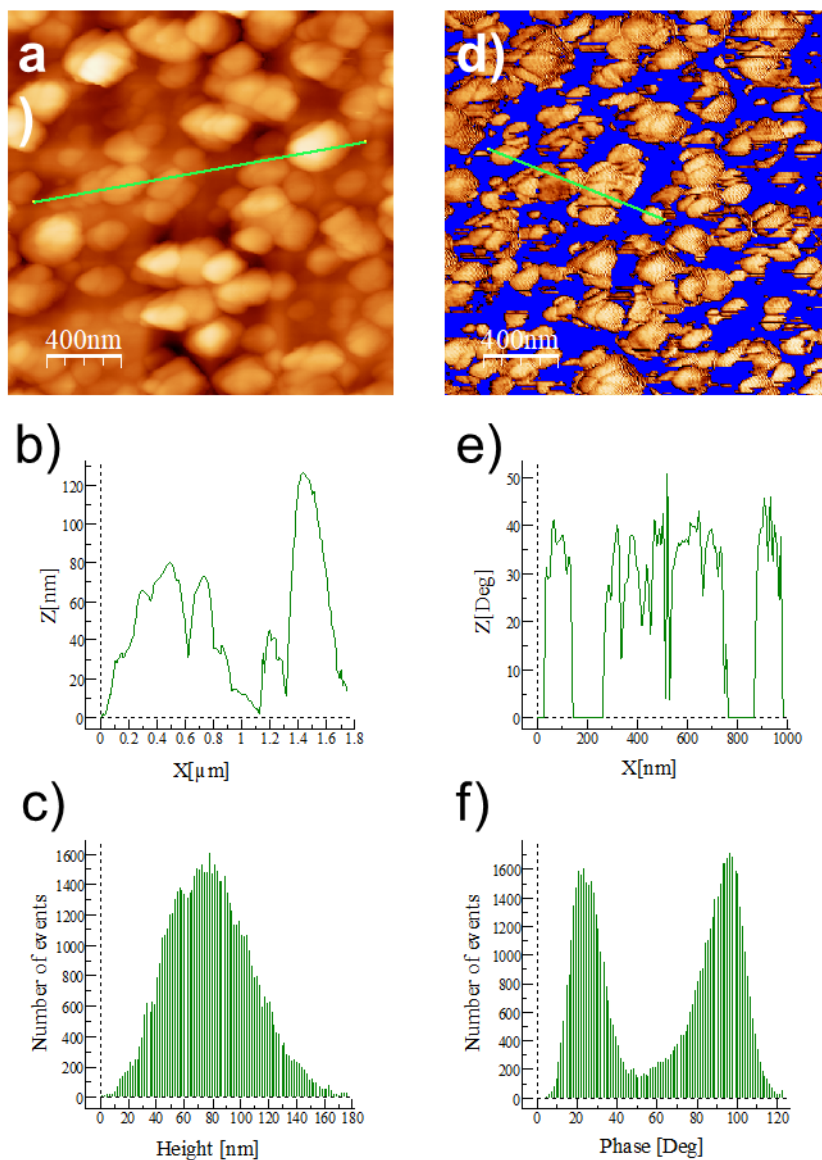


Figure 2. Height (left column) and phase (right column) AFM images of Pd/GC surface obtained by 30 min electrodeposition using PdSO₄ salt at a constant potential of 0.09 V, showing: a) surface topography (z-scale = 198 nm); b) cross-section along the line indicated in the image; c) Pd nanoparticles height distribution; d) phase image, z-scale = 147 Deg; e) cross-section along the line indicated in the image; f) phase angle distribution showing the presence of two chemically different components.

The distribution of Pd nanoparticles heights, Figure 2c, shows that it falls within the range from 10–160 nm, with an average value of 80 nm. At the beginning of the deposition, the first Pd nanoparticles follow the island growth mode on the GC surface. As the Pd deposition continues, these Pd

nanoparticles grow further preferentially in height following layer-by-layer growth mode. That causes a substantial increase of the surface roughness, with its estimated average value of 23. Figure 2d shows phase AFM image, where surface chemical features are independent of surface topography, and Pd nanoparticles are highlighted on the GC substrate.

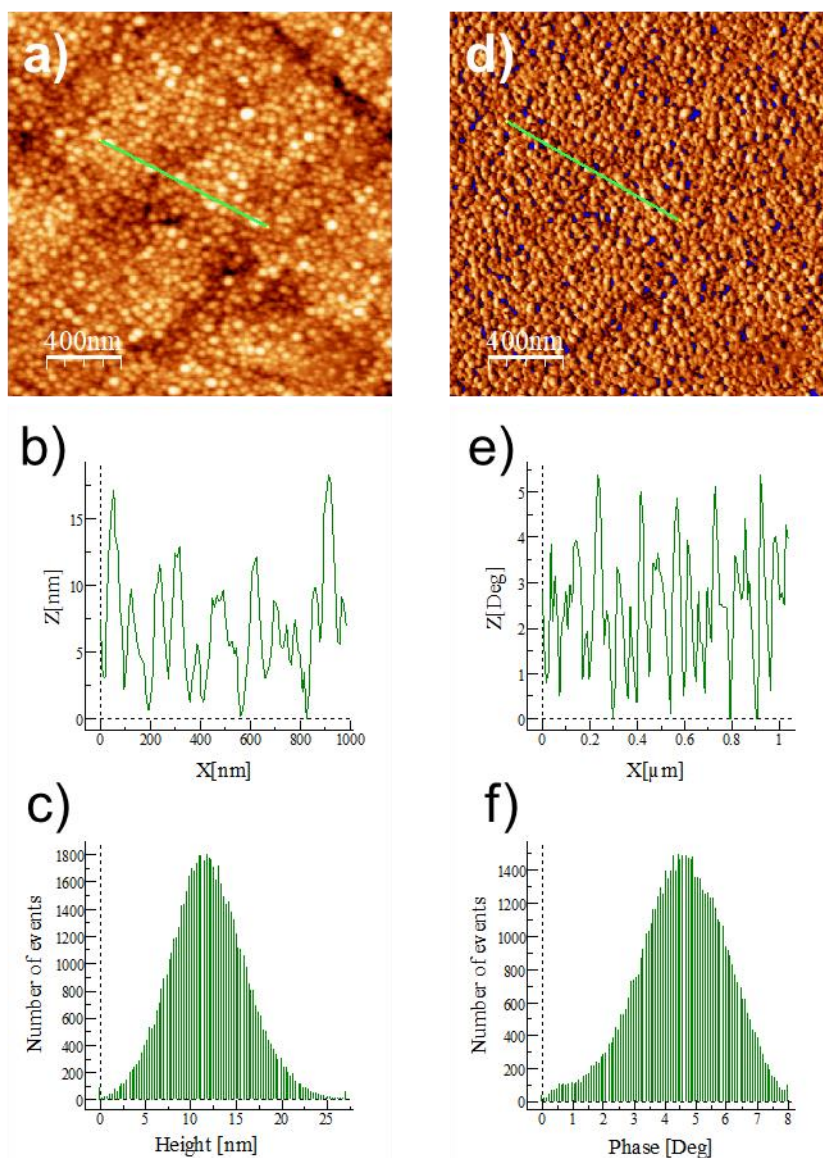


Figure 3. Height (left column) and phase (right column) AFM images of Pd/GC surface obtained by 30 min electrodeposition using PdCl_2 salt at a constant potential of 0.25 V, showing: a) surface topography, (z-scale = 27.4 nm) ; b) cross-section along the line indicated in the image; c) Pd nanoparticles height distribution; d) phase image, z-scale = 8.8 Deg; e) cross-section along the line indicated in the image; f) phase angle distribution showing the presence of the two chemically different components.

The deposited Pd nanoparticles, presented as yellow structures, are clearly distinguished from the uncovered part of the GC substrate, presented as a blue background. This allows a fairly accurate estimate of the coverage given as a percentage of the GC surface area occupied by deposited Pd nanoparticles. Such chemical contrast gives a Pd nanoparticle coverage of $(55 \pm 5)\%$. From the cross-

section in Figure 2e, the lateral size (nm) of the individual Pd nanoparticles (or their agglomerates) are seen in the x-axis, while the phase angle (Deg), reflecting the chemical changes, are seen in the z-axis. Phase angle distribution, Figure 2f, shows two chemically different components, GC and Pd.

Figure 3 shows the height and phase AFM images of the Pd/GC surface prepared by 30 min Pd deposition from (1×10^{-4} M PdCl₂ + 0.05 M H₂SO₄) at a constant potential of 0.25 V.

The height AFM image showing the surface topography, Figure 3a, reveals that densely packed Pd nanoparticles, much smaller than in the previous case, are grown on the GC substrate. Cross-section along the line indicated in the image, Figure 3b, shows that the lateral size of individual and agglomerated Pd nanoparticles ranges from 10-50 nm. The distribution of Pd nanoparticles heights, Figure 3c, shows that it falls within the range from 1-25 nm, with an average value of 12 nm. During the deposition, Pd nanoparticles grow on the GC surface, following the island growth mode. That leads to a moderate increase of the surface roughness, with an estimated average value of 3.3. Figure 3d shows phase AFM image, from which the estimated coverage of the GC surface with the deposited Pd nanoparticles is (95 ± 5)%. The cross-section in Figure 3e illustrates the chemical difference along the line (z-axis), while the x-axis shows the lateral size of the individual Pd nanoparticles. Phase angle distribution, Figure 3f, shows two chemically different components, with a pronounced Pd contribution and a small contribution of the GC substrate.

3.3. XPS analysis of Pd/GC

Figure 4 shows XPS spectra of Pd/GC electrodes prepared by 30 min Pd deposition from the depositing solutions containing two different Pd salts (PdSO₄ and PdCl₂). For both samples, survey spectra show C 1s and O 1s lines originating from the GC substrate, and Pd 3d lines as the most characteristic for Pd deposit. Pd 3p photoelectron lines are also annotated as they overlap with O 1s lines.

It is obvious that for the Pd/GC obtained using the depositing PdSO₄ salt, Figure 4a, peaks associated with Pd are less pronounced, while C 1s peak is higher in intensity as compared to the same peaks for Pd/GC obtained using PdCl₂ salt solution, Figure 4b. Additionally, for the later Pd/GC sample, due to the higher content of Pd on the surface, Pd 3s, Pd 4s, Pd 4p, and Pd 4d overlapped with O 2s peaks, are prominent enough, and therefore annotated in the survey spectra.

For a better insight into the oxidation state of the deposited Pd nanoparticles, high-resolution spectra for the most characteristic Pd 3d lines, are recorded for both Pd/GC samples and presented in Figure 4c and d. For Pd clusters and nanoparticles deposited on various carbon-based materials including carbon foil [46], graphite [47], carbon nanotubes [48], or highly oriented pyrolytic graphite (HOPG) [49], the Pd 3d lines shift towards higher binding energies compared to bare Pd [50], and the line width broadens with decreasing cluster size, due to the interaction with the support. For bare Pd metal, Pd⁰, Pd 3d_{5/2} component appears at 335.4 eV for bare PdO, Pd²⁺, this line appears at 336.8 eV [50].

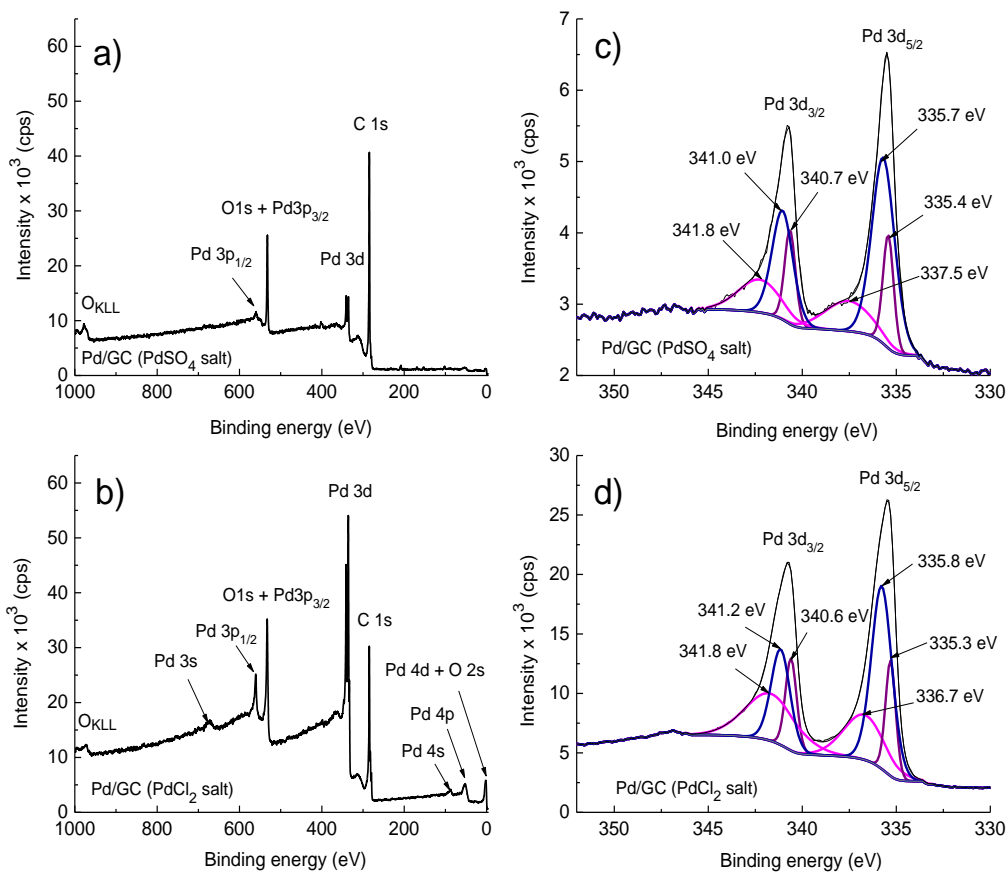


Figure 4. (left column) Survey XPS spectra of Pd/GC obtained using different depositing salts: a) PdSO₄; b) PdCl₂. (right column) High resolution spectra for Pd 3d line for Pd nanoparticles deposited from: c) PdSO₄; d) PdCl₂ salt solutions.

Based on the detailed analysis in ref. [49], both Pd 3d_{5/2} and Pd 3d_{3/2} lines are fitted into three components: surface and bulk component of metallic Pd, and PdO surface oxide component. For comparison, only the binding energies of three Pd 3d_{5/2} components will be analyzed as in most of the papers.

Figure 4c shows the high-resolution spectrum of Pd 3d doublet for Pd/GC obtained after 30 min electrochemical deposition of Pd from PdSO₄ salt solution at the potential of 0.09 V. Pd 3d_{5/2} surface and bulk component at 335.4 eV and at 335.7 eV, respectively, are associated with palladium in its metallic state, while the component at 337.5 eV is associated with PdO. The binding energy of the surface component remains the same, but the bulk component is shifted positively for 0.2 eV compared to bare Pd metal (335.4 eV, given in ref. [50] as a single component). The binding energy of the Pd 3d_{5/2} surface oxide component is shifted positively for 0.6 eV compared to bare PdO powder (336.8 eV in ref. [50]).

Figure 4d shows Pd 3d doublet lines for Pd/GC obtained after 30 min electrochemical deposition of Pd from PdCl₂ salt solution at the potential of 0.25 V. Like in the previous case both Pd 3d_{5/2} and Pd 3d_{3/2} lines are fitted to three components, corresponding to surface and bulk components of metallic Pd and to Pd surface oxide component. The binding energy for the surface component of metallic Pd is close to the value of bare Pd, while the bulk component is shifted to the more positive values for 0.3 eV compared to bare Pd, while the one corresponding to PdO also remains within the error compared ref.

[50]. The difference between the two Pd/GC substrates is that the one obtained from the PdCl₂ salt solution shows a stronger influence of the GC substrate than the one obtained from PdSO₄.

3.4. Electrochemical characterization of Pd/GC electrodes in acid and alkaline solutions

Figure 5 shows cyclic voltammograms of different Pd/GC electrodes recorded in 0.1 M HClO₄ in the potential region from 0.11 V to 1.42 V and in 0.1 M NaOH solution within the potential range from 0.22 V to 1.42 V. Pd/GC electrodes are obtained by the electrochemical palladium deposition from the depositing solutions containing different Pd salts. Depositions are performed at constant potentials, E_{dep} , for 30 min deposition time. Lower potential limits are chosen to avoid hydrogen evolution. Characteristic hydrogen adsorption/desorption processes that occur on the deposited palladium are indicated by the presence of reversible cathodic and anodic peaks at lower potentials [51]. The surface oxidation/reduction peaks of the deposited palladium nanoparticles appear at higher potentials. Besides, both the position and the intensity of Pd oxidation and reduction peaks depend on the upper potential limit due to the gradual and irreversible formation of Pd oxides. For both Pd(poly) [9,52,53], and Pd/GC [25], up to the potential of 1.42 V in both acid and alkaline solution, Pd⁰ is oxidized to Pd²⁺, while with the further increase of the potential the formation of higher Pd oxides occurs. Therefore, these potentials are chosen as the positive potential limit to avoid the formation and irreversible reduction of higher Pd oxides.

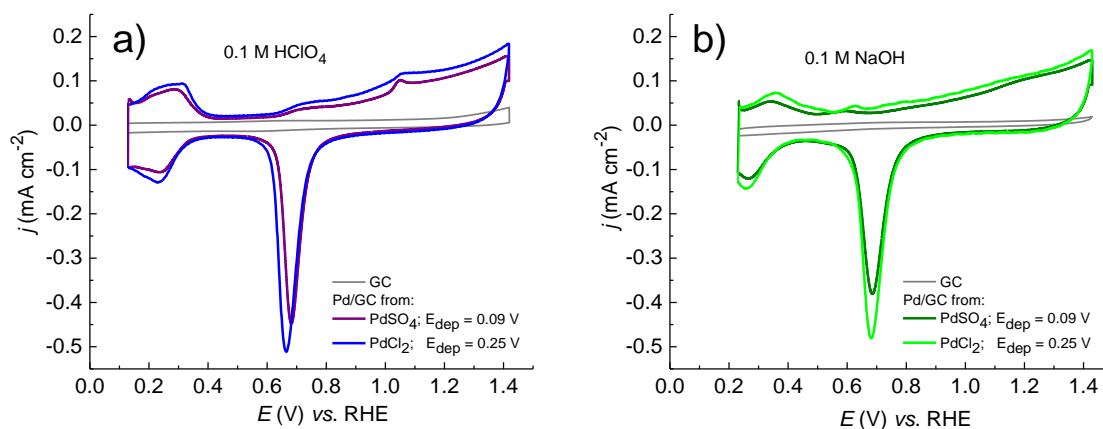


Figure 5. Cyclic voltammograms of Pd/GC electrodes, obtained by 30 min deposition at a constant potential from PdSO₄ and PdCl₂ salt solutions recorded in: a) 0.1 M HClO₄ solution; b) 0.1 M NaOH. CV of a bare GC electrode in both electrolytes are given for comparison. Scan rate was 50 mV s⁻¹.

Figure 5a shows CVs in 0.1 M HClO₄ solution of Pd/GC electrodes obtained by the deposition of palladium from the solutions containing either PdSO₄ or PdCl₂ salt. The CV of Pd/GC electrode obtained after 30 min deposition from PdSO₄ salt solution at 0.09 V, shows that by scanning the potential in the positive direction, palladium oxide formation begins at 0.63 V and proceeds at higher potentials. In the reverse direction, the main palladium reduction peak appears at 0.68 V. CV of Pd/GC electrode obtained by 30 min electrochemical deposition from the solution containing PdCl₂ salt at a constant

potential of 0.25 V shows that palladium oxide formation begins at 0.62 V, while the oxide reduction peak appears at 0.66 V.

Figure 5b shows CVs in 0.1 M NaOH solution of the Pd/GC electrode obtained by 30 min electrochemical deposition from PdSO₄ salt solution at a constant potential of 0.09 V, and from PdCl₂ salt solution at a constant potential of 0.25 V.

In both cases, characteristic hydrogen adsorption/desorption peaks are observed at lower potentials. At higher potentials, the oxidation process begins at approx. 0.67 V following the formation of PdOH_{ads} at slightly lower potentials according to the findings reported in ref. [9]. The main PdO reduction peak appears at approx. 0.68 V.

The type of the Pd salt used for the deposition, as well as the chosen depositing potential influences the growth of Pd particles, the deposit structure, the coverage of the GC substrate by the deposit, as well as the electrochemically active surface area (ECSA) of the obtained Pd/GC electrodes. As shown above, the coverage of the GC substrate with the deposited palladium was estimated from phase AFM images (see Figures 2 and 3). On the other hand, the ECSA is calculated as the ratio between the charge passed during reduction of PdO for Pd/GC and polycrystalline palladium (424 μC/cm²). The charges calculated from the PdO reduction peaks (CVs in Figures 5a and b) for Pd/GC for 30min deposition using PdSO₄ and using PdCl₂ for the upper potential limit of 1.42 V [51,52] are: 584, and 757 μC cm⁻², which gives the ECSAs values of 0.27, and 0.35 cm² respectively.

The ECSA for Pd(poly) was taken from ref. [54], where it was calculated from CO stripping charges, taking into account that the charge for a full CO monolayer adsorbed on bare Pd(poly) substrate was 424 μC cm⁻². The obtained value for Pd(poly) was 445 μC cm⁻², which gives the ECSA of 0.21 cm².

3.5. Oxygen reduction on Pd/GC electrodes in acid and alkaline solutions

Generally, the activity of Pd/GC electrodes for ORR varies depending on the palladium coverage, surface morphology, and the chemical state of the deposited palladium. As mentioned above, these parameters were altered using two different palladium depositing salts, three different deposition potentials, and various deposition times. According to the obtained results for ORR activity, only those for which the best ORR activity is obtained will be presented.

3.5.1. Oxygen reduction on Pd/GC electrodes in 0.1 M HClO₄

For the most active Pd/GC electrodes obtained using different Pd salt solutions, Figure 6 shows ORR polarization curves for different rotation rates, ω , recorded in 0.1 M HClO₄ solution, and corresponding Koutecky–Levich (K-L) plots. Polarization curves for ORR on Pd/GC obtained using PdSO₄ and PdCl₂ salts recorded for five rotation rates are presented in Figure 6a and b, respectively.

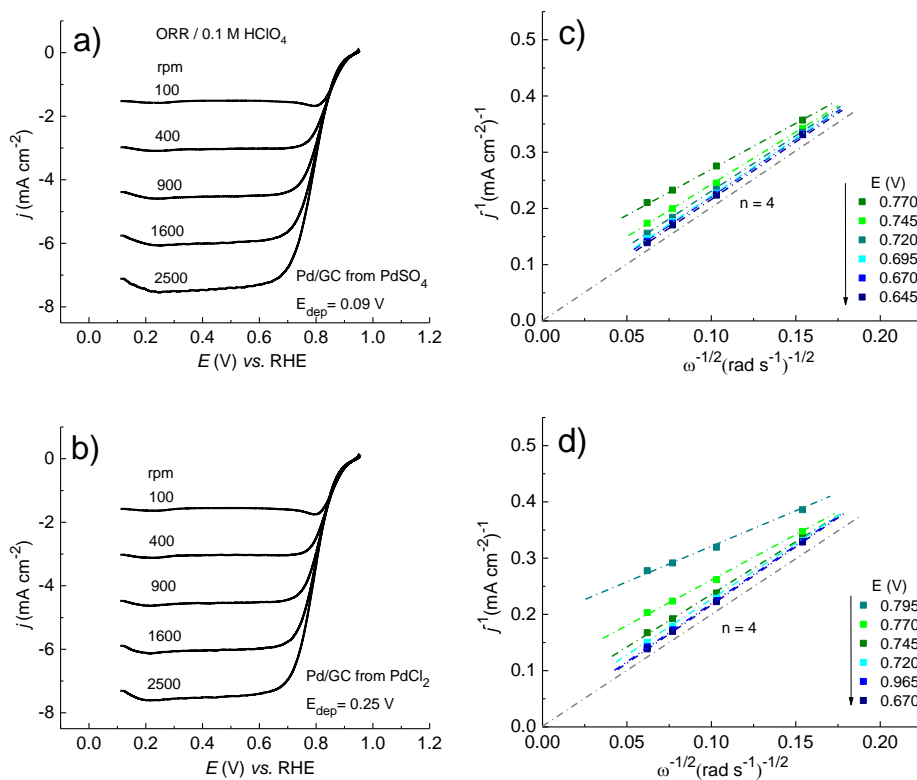


Figure 6. Polarization curves for ORR on 30minPd/GC in 0.1 M HClO₄ obtained using: a) PdSO₄ salt at the deposition potential of 0.09 V, scan rate 50 mV s⁻¹; b) PdCl₂ salt at the deposition potential of 0.25 V, scan rate 50 mV s⁻¹; c, and d) corresponding Koutecky-Levich plots.

ORR polarization curves are analyzed using Koutecky–Levich equation:

$$\frac{1}{j} = \frac{1}{j_k} + \frac{1}{j_l} = \frac{1}{j_k} + \frac{1}{B\omega^{1/2}} \quad (1)$$

where: j , j_k , and j_l are the measured, kinetic, and diffusion-limited current densities, respectively. B is a constant which can be expressed as:

$$B = 0.62nFC_{O_2}D_{O_2}^{2/3}\nu^{-1/6} \quad (2)$$

where: n is the total number of electrons exchanged, F is Faraday's constant (96485 C mol⁻¹); C_{O_2} is the oxygen solubility (1.26×10^{-3} mol L⁻¹[55]), D_{O_2} is the oxygen diffusivity (1.93×10^{-5} cm² s⁻¹ [55]) in 0.1 M HClO₄ solution; ν is the kinematic viscosity (0.01 cm² s⁻¹[56]) of the solution.

Koutecky-Levich plots obtained using the data from polarization curves from Figure 6a and b are presented in Figure 6c and d. The linear dependence of $1/j$ vs. $1/\omega^{1/2}$ diagrams indicates the first-order kinetics toward the concentration of dissolved oxygen. On the other hand, the lack of parallelism indicates that the total number of electrons exchanged depends on the potential. For $1/j = 0$ and $1/\omega^{1/2} = 0$, the total number of electrons exchanged is four in both cases indicating a 4e-series reaction pathway.

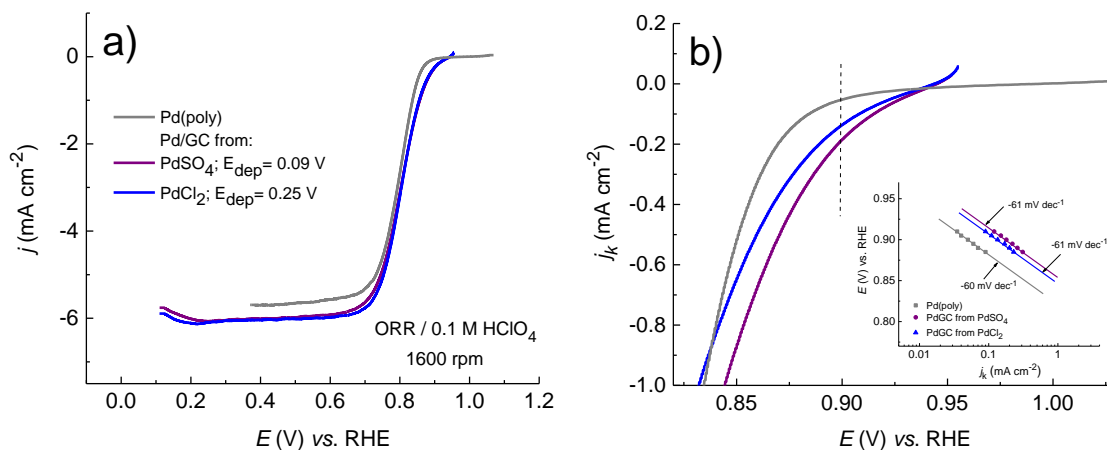


Figure 7. Comparison of the catalytic activity for ORR in oxygen saturated 0.1 M HClO₄ solution of different Pd/GC electrodes obtained by the deposition of palladium from PdSO₄ and PdCl₂ salt solutions and Pd(poly): a) current densities on polarization curves are given with respect to the geometric area of the GC electrode; b) current densities in the activation control region are given with respect to the ECSA; insert shows corresponding Tafel plots.

ORR activities of different Pd/GC electrodes are compared and analyzed in Figure 7, using polarization curves recorded with the same rotation rate of 1600 rpm (taken from Figure 6). Figure 7a shows that in both cases, ORR begins in the potential range of PdO formation (see CVs in Figure 5a). To get a better insight into the catalytic activity for ORR, polarization curves for the most active Pd/GC electrodes obtained using two different Pd salts can be compared to the one for polycrystalline Pd [9], which is also presented. The ORR initial potential (for $j_k = 0$) is 0.94 V for both Pd/GC obtained by palladium deposition from PdSO₄ and PdCl₂ salts. Concerning the initial potentials, the ORR activity of Pd/GC electrode obtained using PdCl₂ salt, exceeds the activity of Pd(poly) for 30 mV (0.91 V [9]). Figure 7b shows kinetic currents in the activation control region, where the current densities are given with respect to the ECSA, and from which the corresponding Tafel slopes are calculated as shown in the insert. For Pd/GC electrodes the Tafel slopes of -60 mV dec^{-1} are characteristic for Pd-based catalyst [19,51], meaning that the rate-determining step is the exchange of the first electron.

The specific activity (SA) for ORR at a given potential is calculated according to the following equation:

$$SA = I_k / ECSA \quad (3)$$

where: I_k is the kinetic current at a given potential, and ECSA is the electrochemically active surface area of the electrode.

The kinetic parameters for ORR on different Pd/GC catalysts in 0.1 M HClO₄ solution at 1600 rpm involving Tafel slope, half-wave potential and the specific activity at 0.90 V are given in Table 1.

Table 1. Kinetic parameters for ORR on Pd/GC in 0.1M HClO₄ solution

Catalyst	ECSA (cm ²)	Tafel slope (mV dec ⁻¹)	E _{1/2} (V)	SA at 0.90 V (mA cm ⁻²)
Pd/GC from PdSO ₄	0.27	-61	0.810	-0.19
Pd/GC from PdCl ₂	0.35	-61	0.811	-0.13
Pd(poly)	0.21	-60	0.793	-0.05

3.5.2. Oxygen reduction on Pd/GC electrodes in 0.1 M NaOH solution

Figure 8 shows polarization curves for ORR on Pd/GC electrodes recorded in 0.1 M NaOH solution in the cathodic direction for five rotation rates and corresponding Koutecky-Levich plots. K-L plots are linear and mainly parallel, indicating the first-order kinetics relative to the concentration of dissolved oxygen (for 0.1 M NaOH, C_{O_2} is 1.22×10^{-3} mol L⁻¹ [56], and D_{O_2} is 1.90×10^{-5} cm² s⁻¹ [56]). Although the total number of electrons exchanged slightly varied potential, which can be seen by the non-parallelism in K-L plots, the total number of electrons exchanged is four.

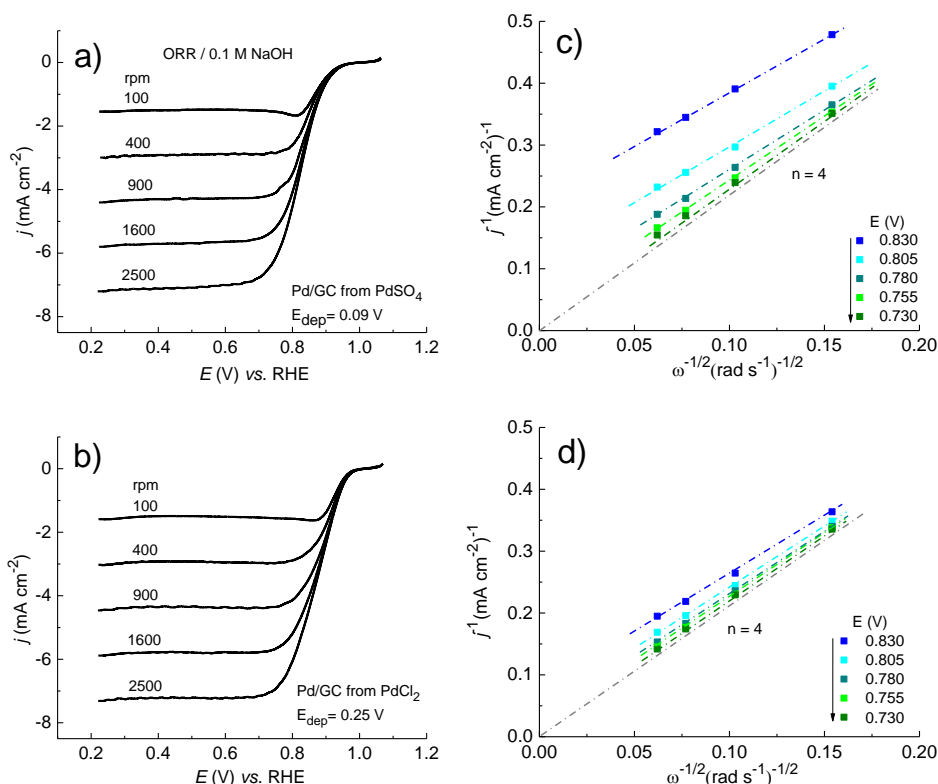


Figure 8. Polarization curves for ORR on Pd/GC in 0.1 M NaOH obtained using: a) PdSO₄ salt, 30 min deposition at 0.09 V, scan rate 50 mV s⁻¹; b) PdCl₂ salt, 30 min deposition at 0.25 V, scan rate was 50 mV s⁻¹; c, and d) corresponding Koutecky-Levich plots.

Figure 9 shows polarization curves for ORR on different Pd/GC electrodes for the same rotation rate of 1600 rpm (taken from Figure 8.). The polarization curve for Pd(poly) is given for comparison.

Figure 9a shows that ORR begins at 1.02 V for Pd/GC from PdSO₄, and at 1.04 V from PdCl₂, with the later one 60 mV more positive than for bare Pd(poly), which is 0.98 V. Figure 9 b shows the same polarization curves in the activation control region, where the current densities are given with respect to the ECSA. The insert shows that Tafel slope for Pd/GC electrode obtained using PdSO₄ salt is -60 mV dec⁻¹, which is equal to the slope for Pd(poly) in ref. [9], indicating that the exchange of the first electron is the rate-determining step. On the other hand, Tafel slope for Pd/GC electrode obtained using PdCl₂ salt is -0.47 mV dec⁻¹, indicating a faster reaction kinetics.

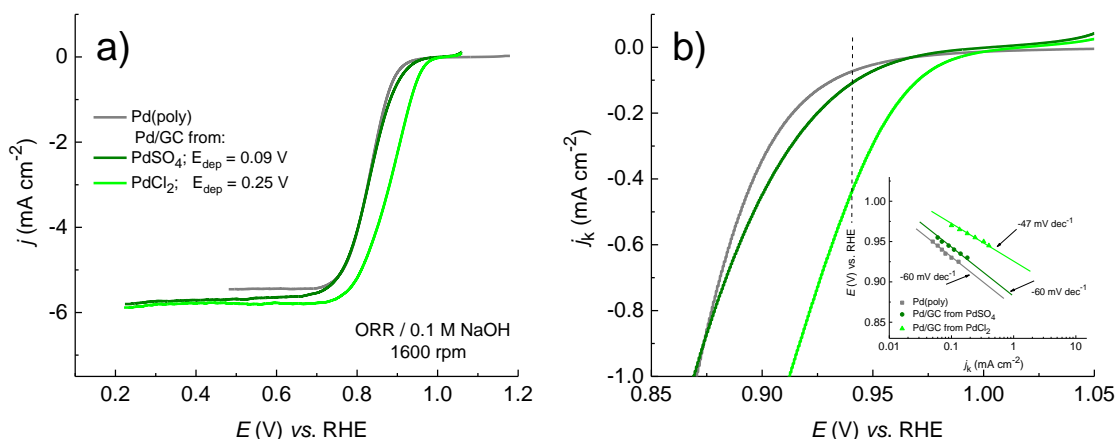


Figure 9. Comparison of the catalytic activity of Pd/GC electrodes obtained using PdSO₄ and PdCl₂ salts, and Pd(poly) for ORR in 0.1 M NaOH: a) a) current densities on polarization curves are given with respect to the geometric area of the GC electrode; b) current densities in the activation control region are given with respect to the ECSA; insert shows corresponding Tafel plots.

The kinetic parameters for ORR on different Pd/GC catalysts in 0.1 M NaOH solution at 1600 rpm involving Tafel slope, half-wave potential and the specific activity at 0.94 V are given in Table 2.

Table 2. Kinetic parameters for ORR on Pd/GC in 0.1 M NaOH solution

Catalyst	ECSA (cm ²)	Tafel slope (mV dec ⁻¹)	E _{1/2} (V)	SA at 0.94 V (mA cm ⁻²)
Pd/GC from PdSO ₄	0.27	-60	0.828	-0.10
Pd/GC from PdCl ₂	0.35	-47	0.882	-0.43
Pd(poly)	0.21	-60	0.827	-0.07

For all Pd/GC electrodes, presented in this work, ORR occurs through a 4-series pathway, indicating a reaction mechanism similar to that of polycrystalline palladium. A higher ORR activity concerning the initial potential can be ascribed to the presence of more Pd surface active sites on the deposited Pd nanoparticles than on Pd(poly). Among all investigated electrodes, the highest ORR activity is achieved for Pd/GC obtained after 30 min Pd deposition from PdCl₂ depositing solution. The

activity of the same electrode in acid and alkaline solutions can be compared taking into account the difference between the ORR initial potentials and corresponding equilibrium potentials. Namely, the equilibrium potential for ORR is 1.23 V (vs. SHE) [57], which according to the Nernst equation gives the values of 1.22 V in 0.1 M HClO₄, and 1.23 V in 0.1 M NaOH solution. The values obtained for the initial potentials for ORR on Pd/GC electrode obtained using PdCl₂ salt are 0.94 V in 0.1 M HClO₄, and 1.04 V in 0.1 M NaOH solution are lower than the corresponding equilibrium potentials. On the other hand, the difference between the initial and equilibrium potentials is lower for an alkaline solution, meaning that the obtained Pd/GC electrodes show higher activity in alkaline than in acid solution. This can be explained by the oxidation of Pd nanoparticles to PdOH, with OH taking part in ORR in alkaline solution. Although the oxidation/reduction of Pd nanoparticles for both Pd/GC obtained using either PdSO₄ or PdCl₂ salts, occurs in almost the same potential region, the one obtained from PdCl₂ shows higher coverage and lower roughness which most likely provide sterically more favorable Pd (or PdOH) surface sites for the adsorption of molecular oxygen and its further reduction.

4. CONCLUSIONS

Pd nanoparticles were electrochemically deposited on glassy carbon using PdSO₄ and PdCl₂ salt solutions at various deposition potentials and times. Pd/GC electrodes that showed the best ORR catalytic activity, were examined in detail. XPS spectra of as-prepared Pd/GC electrodes revealed that in both cases the deposited Pd nanoparticles consist of a mixture of metallic Pd, and Pd oxide. AFM analysis revealed 55% coverage of the GC substrate with the palladium nanoparticles when deposited using PdSO₄ salt, and full coverage when deposited using PdCl₂ salt. The respective ECSAs estimated from the PdO reduction CV peaks were 0.27 and 0.3 cm², respectively, exceeding the geometric area of the GC substrate (0.196 cm²). Concerning the initial potential, Pd/GC electrode obtained using PdCl₂ salt has shown the best ORR activity, exceeding that of Pd(poly), which was ascribed to the presence of PdOH as active surface sites favorable for the adsorption of molecular oxygen and its further reduction through 4e-series pathway.

FUNDING SOURCES

The authors would like to thank the Ministry of Education, Science and Technological Development of Republic of Serbia (Grant No: 451-03-68/2022-14/200026) for financial support.

References

1. F.H.B. Lima, J. Zhang, M.H. Shao, K. Sasaki, M.B. Vukmirovic, E.A. Ticianelli, R.R. Adzic, *J. Phys. Chem. C*, 111 (2007) 404.
2. A. Kulkarni, S. Siahrostami, A. Patel, J.K. Nørskov, *Chem. Rev.*, 118 (2018) 2302.
3. N.M. Marković, R.R. Adžić, B.D. Cahan, E.B. Yeager, *J. Electroanal. Chem.*, 377 (1994) 249.
4. N.M. Markovic, H.A. Gasteiger, P.N. Ross Jr, *J. Phys. Chem.*, 100 (1996) 6715.
5. A.M. Gómez-Marín, R. Rizo, J.M. Feliu, *Catal. Sci. Technol.*, 4 (2014) 1685.
6. S. Kondo, M. Nakamura, N. Maki, N. Hoshi, *J. Phys. Chem.*, 113 (2009) 12625.
7. S. Štrbac, *Electrochim. Acta*, 56 (2011) 1597.

8. Lj.M. Vračar, D.B. Šepa, A. Damjanović, *J. Electrochem. Soc.*, 133 (1986) 1835.
9. I. Srejić, Z. Rakočević, M. Nenadović, S. Štrbac, *Electrochim. Acta*, 169 (2015) 22.
10. M.-H. Shao, T. Huang, P. Liu, J. Zhang, K. Sasaki, M.B. Vukmirovic, R.R. Adzic, *Langmuir*, 22 (2006) 10409.
11. J.B. Joo, Y.J. Kim, W. Kim, N.D. Kim, P. Kim, Y. Kim, J. Yi, *Korean J. Chem. Eng.*, 25 (2008) 770.
12. M. Shao, Q. Chang, J.-P. Dodelet, R. Chenitz, *Chem. Rev.*, 116 (2016) 3594.
13. T. Wang, A. Chutia, D.J.L. Brett, P.R. Shearing, G. He, G. Chai, I.P. Parkin, *Energy Environ. Sci.*, 14 (2021) 2639.
14. Y-F. Yang, Y-H. Zhou, C-S. Cha, *Electrochim. Acta*, 40 (1995) 2579.
15. L. Jiang, A. Hsu, D. Chu, R. Chen, *J. Electrochem. Soc.*, 156 (2009) B370.
16. L. Jiang, A. Hsu, D. Chu, R. Chen, *J. Electrochem. Soc.*, 156 (2009) B643.
17. H. Erikson, A. Sarapuu, J. Solla-Gullón, K. Tammeveski, *J. Electroanal. Chem.*, 780 (2016) 327.
18. M. Lüsi H. Erikson, A. Sarapuu, K. Tammeveski, A. Treshchalov, A. Kikas, V. Kisand, A. Tamm, H-M. Piirsoo, J. Arüvali, J. Solla-Gullón, J.M. Feliu, *Electrochim. Acta*, 394 (2021) 139132.
19. H. Erikson, M. Liik, A. Sarapuu, V. Sammelselg, K. Tammeveski, *Electrochim. Acta*, 88 (2013) 513.
20. H. Erikson, A. Kasikov, C. Johans, K. Kontturi, K. Tammeveski, A. Sarapuu, *J. Electroanal. Chem.*, 652 (2011) 1.
21. M. Lüsi, H. Erikson, M. Merisalua, M. Rähn, V. Sammelselg, K. Tammeveski, *J. Electroanal. Chem.*, 834 (2019) 223.
22. H. Erikson, A. Sarapuu, K. Tammeveski, J. Solla-Gullón, J.M. Feliu, *Electrochem. Commun.*, 13 (2011) 734.
23. H. Erikson, A. Sarapuu, N. Alexeyeva, K. Tammeveski, J. Solla-Gullón, J.M. Feliu, *Electrochim. Acta*, 59 (2012) 329.
24. M. Lüsi, H. Erikson, A. Sarapuu, K. Tammeveski, J. Solla-Gullón, J.M. Feliu, *Electrochem. Commun.*, 64 (2016) 9.
25. L. Xiao, L. Zhuang, Y. Liu, J. Lu, H.D. Abruña, *J. Am. Chem. Soc.*, 131 (2009) 602.
26. A. Chen, C. Ostrom, *Chem. Rev.*, 115 (2015) 11999.
27. M. Favaro, S. Agnoli, L. Perini, C. Durante, A. Gennaro, G. Granozzi, *Phys. Chem. Chem. Phys.*, 15 (2013) 2923.
28. A.M. Trzeciak, P. Wojcik, R. Lisiecki, Y. Gerasymchuk, W. Streck, J. Legendziewicz, *Catalysts*, 9 (2019) 319
29. M. Asnavandi, B.H.R. Suryanto, C. Zhao, *RSC Advances*, 5 (2015) 74017.
30. A. Hernández Creus, Y. Gimeno, P. Díaz, L. Vázquez, S. González, R.C. Salvarezza, A.J. Arvia, *J. Phys. Chem. B*, 108 (2004) 10785.
31. O. Corduneanu, V.C. Diculescu, A.-M. Chiorcea-Paquim, A.-M. Oliveira-Brett, *J. Electroanal. Chem.*, 624 (2008) 97.
32. S. Bliznakov, M. Vukmirovic, E. Sutter, R. Adzic, *Maced. J. Chem. Chem. Eng.*, 30 (2011) 19.
33. S.T. Bliznakov, M.B. Vukmirovic, L. Yang, E.A. Sutter, R.R. Adzic, *J. Electrochem. Soc.*, 159 (2012) F501.
34. M. Rezaei, S. Hadi Tabaian, D.F. Haghshenas, *Electrochim. Acta*, 59, (2012) 360.
35. I.E. Espino-López, M. Romero-Romo, M.G. Montes de Oca-Yemha, P. Morales-Gil, M.T. Ramírez-Silva, J. Mostany, M. Palomar-Pardavé, *J. Electrochem. Soc.*, 166 (2019) D3205.
36. L. Juárez-Marmolejo, B. Maldonado-Teodocio, M.G. Montes de Oca-Yemha, M. Romero-Romo, M.T. Ramírez-Silva, E.M. Arce-Estrada, P. Morales-Gil, J. Mostany, M. Palomar-Pardavé, *J. Phys. Chem. B*, 124 (2020) 3973.
37. H. Meng, D. Zeng, F. Xie, *Catalysts*, 5 (2015) 1221.
38. B. K. Jena, S.C. Sahu, B. Satpati, R.K. Sahu, D. Behera, S. Mohanty, *Chem. Commun.*, 47 (2011) 3796.
39. R. Zhou, W. Zhou, H. Zhang, Y. Du, P. Yang, C. Wang, J. Xu, *Nanoscale Res. Lett.*, 6 (2011) 381.

40. J. Yu, T. Fujita, A. Inoue, T. Sakurai, M. Chen, *Nanotechnology*, 21 (2010) 085601.
41. M. Kang, Y. Yang, J.H. Shim, S.C. Lee, Y. Lee, C. Lee, *Electroanalysis*, 25 (2013) 2691.
42. G.F. Alvarez, M. Mamlouk, S.M. Senthil Kumar, K. Scott, *J. Appl. Electrochem.*, 41 (2011) 925.
43. P. Mayer, R. Holze, *J Solid State Electrochem.*, 5 (2001) 402.
44. R. Hoyer, L.A. Kibler, D.M. Kolb, *Electrochim. Acta*, 49 (2003) 63.
45. J. Tang, M. Petri, L.A. Kibler, D.M. Kolb, *Electrochim. Acta*, 49 (2005) 125.
46. T.T.P. Cheung, *Surf. Sci. Lett.*, 127 (1983) L129.
47. G.K. Wertheim, S.B. DiCenzo, D.N.E. Buchanan, *Phys. Rev. B*, 33 (1986) 5384.
48. A. Felten, J. Ghijssen, J.-J. Pireaux, W. Drube, R.L. Johnson, D. Liang, M. Hecq, G. Van Tendeloo, C. Bittencourt, *Micron*, 40 (2009) 74.
49. L. Chen, A. Yelon, E. Sacher, *J. Phys. Chem. C*, 115 (2011) 7896.
50. M. Brun, A. Berthet, J. Bertolini, *J. Electron Spectros. Relat. Phenomena*, 104 (1999) 55.
51. N. Tateishi, K. Yahikozawa, K. Nishimura, M. Suzuki, Y. Iwanaga, M. Watanabe, E. Enami, Y. Matsuda, Y. Takasu, *Electrochim. Acta*, 36 (1991) 1235.
52. M. Grdeń, M. Łukaszewski, G. Jerkiewicz, A. Czerwiński, *Electrochim. Acta*, 53 (2008) 7583.
53. T. Chierchie, C. Mayer, W.J. Lorenz, *J. Electroanal. Chem.*, 135 (1982) 211.
54. S. Štrbac, A. Maksić, Z. Rakočević, *J. Electroanal. Chem.*, 823 (2018) 161.
55. N. Wakabayashi, M. Takeichi, M. Itagaki, H. Uchida, M. Watanabe, *J. Electroanal. Chem.*, 574 (2005) 339.
56. J. Zagal, P. Bindra, E. Yeager, *J. Electrochem. Soc.*, 127 (1980) 1506.
57. A.B. Anderson, T. V. Albu, *J. Am. Chem. Soc.*, 121 (1999) 11855.

© 2022 The Authors. Published by ESG (www.electrochemsci.org). This article is an open access article distributed under the terms and conditions of the Creative Commons Attribution license (<http://creativecommons.org/licenses/by/4.0/>).